Tunable Phonon Polaritons in Atomically Thin van der Waals Crystals of Boron Nitride

Citation: Dai, S., Z. Fei, Q. Ma, A. S. Rodin, M. Wagner, A. S. McLeod, M. K. Liu, et al. "Tunable Phonon Polaritons in Atomically Thin van Der Waals Crystals of Boron Nitride." Science 343, no. 6175 (March 7, 2014): 1125–1129.

As Published: http://dx.doi.org/10.1126/science.1246833

Publisher: American Association for the Advancement of Science (AAAS)

Persistent URL: http://hdl.handle.net/1721.1/90317

Version: Author's final manuscript: final author's manuscript post peer review, without publisher's formatting or copy editing

Tunable phonon polaritons in atomically thin van der Waals crystals of boron nitride

Authors: S. Dai[1], Z. Fei[1], Q. Ma[2], A. S. Rodin[3], M. Wagner[1], A. S. McLeod[1], M. K. Liu[1], W. Gannett[4,5], W. Regan[4,5], K. Watanabe[6], T. Taniguchi[6], M. Thiemens[7], G. Dominguez[8], A. H. Castro Neto[3,9], A. Zettl[4,5], F. Keilmann[10], P. Jarillo-Herrero[2], M. M. Fogler[1], D. N. Basov[1*]

Affiliations:

[1]Department of Physics, University of California, San Diego, La Jolla, California 92093, USA

[2]Department of Physics, Massachusetts Institute of Technology, Cambridge, Massachusetts 02139, USA

[3]Department of Physics, Boston University, Boston, Massachusetts 02215, USA

[4]Department of Physics and Astronomy, University of California, Berkeley, Berkeley, California 94720, USA

[5]Materials Sciences Division, Lawrence Berkeley National Lab, Berkeley, California 94720, USA

[6]National Institute for Materials Science, Namiki 1-1, Tsukuba, Ibaraki 305-0044, Japan

[7]Department of Chemistry and Biochemistry, University of California, San Diego, La Jolla, California 92093, USA

[8]Department of Physics, California State University, San Marcos, San Marcos, California 92096, USA

[9]Graphene Research Centre and Physics Department, National University of Singapore, 6 Science Drive 2, Singapore 117546, Singapore

[10]Ludwig-Maximilians-Universität and Center for Nanoscience, 80539 München, Germany

*Correspondence to: dbasov@physics.ucsd.edu

Abstract: van der Waals heterostructures assembled from atomically thin crystalline layers of diverse two-dimensional solids are emerging as a new paradigm in the physics of materials. We use infrared (IR) nano-imaging to study the properties of surface phonon polaritons in a representative van der Waals crystal, hexagonal boron nitride (hBN). We launched, detected and imaged the polaritonic waves in real space and altered their wavelength by varying the number of crystal layers in our specimens. The measured dispersion of polaritonic waves was shown to be governed by the crystal thickness according to a scaling law that persists down to a few atomic layers. Our results are likely to hold true in other polar van der Waals crystals and may lead to their new functionalities.

Main Text: Layered van der Waals (vdW) crystals consist of individual atomic planes weakly coupled by vdW interaction, similar to graphene monolayers in bulk graphite (*1-3*). These materials can harbor superconductivity (*2*) and ferromagnetism (*4*) with high transition temperatures, emit light (*5-6*) and exhibit topologically protected surface states (*7*), among many other effects (*8*). An ambitious practical goal (*9*) is to exploit atomic planes of van der Waals

crystals as building blocks of more complex artificially stacked structures where each such block will deliver layer-specific attributes for the purpose of their combined functionality (*3*). Here we explore the behavior of phonon polaritons in hexagonal boron nitride (hBN), a representative vdW crystal. The phonon polaritons are collective modes that originate from coupling of photons with optical phonons (*10*) in polar crystals that have been investigated in the context of energy transfer (*11, 12*), coherent control of the lattice (*13*), ultra-microscopy (*14, 15*), "superlensing" (*16*) and metamaterials (*17, 18*). Tunable phonon polaritons that we discovered in hBN by direct infrared (IR) nano-imaging set the stage for the implementation of all these appealing concepts in vdW heterostructures. Polaritonic effects reported here are most certainly generic to other classes of polar vdW solids since these materials commonly show optical phonons. The hBN investigate here stands out in view of its light constituent elements yielding the superior strength of phonon resonances that span a broad region of technologically important IR band.

IR nano-imaging and Fourier transform infrared nano-spectroscopy (nano-FTIR) experiments were performed at UCSD using a scattering-type scanning near-field optical microscope (s-SNOM) (*19*). The physics of polariton imaging using s-SNOM is akin to nano-imaging of surface plasmons (*20, 21*) (Fig. 1A). In short, we illuminated the metalized tip of an atomic force microscope (AFM) with an IR beam. We used quantum cascade lasers (QCLs) with tunable frequency $\omega = 1/\lambda_{IR}$, where λ_{IR} is IR beam wavelength and a broad-band difference frequency generation (DFG) laser system (*22*). Our AFM tip with curvature radius $a \approx 25$ nm is polarized by the incident IR beam. The light momenta imparted by the tip extend to the typical range of momenta supporting phonon polaritons in hBN (Fig. 2E). Therefore, the strong electric field between the tip and sample provides the necessary momentum to launch polariton waves of wavelength λ_p that propagate radially outward from the tip along the hBN surface. AFM tips exploited in our nano-spectroscopy instrument are commonly referred to as "optical antennas" (*23*): an analogy that is particularly relevant to describe the surface wave launching function of the tip. Upon reaching the sample edge, polaritonic waves are reflected back, forming a standing wave between the tip and hBN edge. As the tip is scanned towards the edge, the scattering signal collected from underneath the tip reveals oscillations with the period of $\lambda_p/2$.

Representative nano-imaging data are displayed in Fig. 1B and Fig. 1D-F where we plot the normalized near-field amplitude $s(\omega) = s_{hBN}(\omega)/s_{Au}(\omega)$ at several IR frequencies in the 1550 to 1580 cm^{-1} range. Here, $s_{hBN}(\omega)$ and $s_{Au}(\omega)$ are the scattering amplitudes for, respectively, the sample and the reference (Au-coated wafer) (*19*). The amplitudes were demodulated at the third or the fourth harmonic of the tapping frequency to isolate the genuine near field signal (*23*). The images in Fig. 1B-F were taken for a tapered hBN crystal of thickness $d = 256$ nm. They reveal a hatched pattern of periodic maxima — fringes — of $s(\omega)$ running parallel to the edges, with the "hot spots" located where the two or more fringes intersect. We observed similar fringe patterns in other hBN samples, including those that are only a few atomic layers thick (Fig. 1G). Such patterns are readily accounted for (Fig. 1C) within a phenomenological theory that considers reflections from the tapered edges (*19*).

Data in Fig. 1 allow one to obtain the polariton wavelength λ_p simply by doubling the fringe period and the corresponding momentum can be calculated as $q = 2\pi/\lambda_p$. We used two approaches to determine the dispersion relation $q = q(\omega)$ of the polaritons. One method (*15, 20, 21*) is to analyze the periodicity of fringes at discrete frequencies of the IR source (Fig. 1B, D-G). We have complemented this procedure with a technique capable of capturing the entire dispersion in the course of one single scan of our nanoscope. We executed this line scan on an

hBN crystal with a large surface area to ensure that the $L = 0$ boundary is the principal reflector for the tip-launched polaritons (Fig. 2A). Such a line scan (Fig. 2A-B, D) is comprised of a series of broad-band nano-FTIR spectra taken at every pixel. Starting in the region of unobscured SiO_2 substrate ($L < 0$) and continuing through the hBN crystal ($L > 0$), we combined the spectra from all pixels along the line scan and thus obtained a two-dimensional map $s(L, \omega)$ shown in Fig. 2B. In the plot, we observed a series of resonances that systematically vary with frequency ω and the distance from the sample edge L. The nano-FTIR spectra from three representative positions are shown in Fig. 2C. Each of the frames in Fig. 2C and each pixel in Fig. 2B unveil phonon polaritons in the frequency domain. The momentum q corresponding to each ω in this map can be found from the fringe periodicity along the ω = constant cut. Therefore, a single line scan is sufficient to extract the complete dispersion profile of any surface mode.

The two approaches for mapping the surface wave dispersion produced consistent results (triangles in Fig. 2B were obtained from monochromic imaging). The broad-band line scan data (dots in Fig. 2E) allowed us to probe the dispersion in the $\omega - q$ parameter space (1430 to 1530 cm^{-1}) that cannot be investigated through the single-frequency imaging because of unavailability of proper QCLs. The experimental data for phonon polariton dispersion in Fig. 2E are in excellent agreement with the modeling results. Briefly, the surface polaritons correspond to the divergences of the reflectivity $r_p(q + i\kappa, \omega)$ of the system at complex momenta $q + i\kappa$ (*10*). For $\lambda_p \ll \lambda_{IR}$, we derived the analytical formula for polariton dispersion (*19*):

$$q(\omega) + i\kappa(\omega) = -\frac{\psi}{d}\left[\arctan\left(\frac{\varepsilon_a}{\varepsilon_\perp \psi}\right) + \arctan\left(\frac{\varepsilon_s}{\varepsilon_\perp \psi}\right) + \pi l\right], \quad \psi = \frac{\sqrt{\varepsilon_{//}}}{i\sqrt{\varepsilon_\perp}}, \qquad (1)$$

where $\varepsilon_a(\omega)$, $\varepsilon_\perp(\omega)$, $\varepsilon_{//}(\omega)$ and $\varepsilon_s(\omega)$ are the dielectric functions of air, hBN (for directions perpendicular and parallel to the *c*-axis), and SiO_2 substrate, respectively. The propagating modes correspond only to those integer l (if any) for which the loss factor $\gamma = \alpha\kappa/q$ is positive and less than unity. Parameter $\alpha = \pm$ is the sign of the group velocity $d\omega/dq$ (*19*). An instructive way to visualize both the dispersion and the damping is via a false color plot of Im $r_p(q, \omega)$ (*19, 24*) at real q and ω (Fig. 2E). Our data line up with the topmost of these curves, which corresponds to the principal $l = 0$ branch (*19*) in Eq. 1.

Additional insights into the photonic and polaritonic properties of hBN were obtained by analyzing the frequency dependence of the nano-FTIR spectra. We collected the spectrum in Fig. 2F far away from the hBN edges where the surface waves are damped and the scattering amplitude signal is solely governed by the local interaction with the phonon resonances (*25*). Two of these resonances centered around 770 cm^{-1} and 1370 cm^{-1} are due to the *c*-axis and the in-plane phonon modes of hBN, respectively (*26, 27*). The hump-dip feature around 1100 cm^{-1} originates from the SiO_2 substrate (*28*): a consequence of a partial transparency of our specimen. The quantitative relation between this spectrum, the reflectivity $r_p(q, \omega)$, and the fundamental phonon modes can be established by numerical modeling of the tip-sample interaction (*19*). The right plot of Fig. 2F indicates that our model captures the gross features of the data. Moreover, the hBN is an example of a natural hyperbolic material (*29*): a crystal possessing the in-plane and out-of-plane components of the dielectric tensor having the opposite signs so that $\mathrm{Re}\,\varepsilon_\perp \cdot \mathrm{Re}\,\varepsilon_{//} < 0$. Hyperbolic regions are marked in green in Fig. 2F.

The layered nature of vdW materials, including hBN, facilitates the control of both the wavelength and the amplitude of polaritonic waves by varying the thickness d of the specimens. Representative line profiles (Fig. 3A) for specimens with d in the range of 150−250 nm were taken normal to the crystal edge at $L = 0$. The thickness was measured simultaneously with the scattering amplitude through the AFM topography. All fringe profiles share the same line form with a prominent peak close to the edge followed by weaker peaks that are gradually suppressed away from the edge. The oscillation period, equal to $\lambda_p/2$ (arrows in Fig. 3A), systematically decreases as the samples become thinner. This scaling extends down to a few atomic layers (Fig. 3B-C).

The measured polariton wavelength (Fig. 3E) agrees with the theoretical predictions (Fig. 3D). For λ_p smaller than about one half of $\lambda_{IR} = 7.1$ μm, the polariton wavelength scales linearly with the crystal thickness d, in agreement with Eq. 1; at larger λ_p the linear law shows signs of saturation, also in accord with our model (inset of Fig. 3E). Experimentally, the phonon polaritons display thickness-tunability persisting down to three atomic layers (Fig. 3B-C). We detected polaritons in even thinner samples (bilayer and monolayer hBN). However, the quantitative analysis of these latter data is complicated because of the increasing role of the substrate in the polaritonic response that calls for further experiments on suspended membranes.

Similar to surface plasmons, the phonon polaritons allow one to confine and control electromagnetic energy at the nanoscale (*30*). In fact, the line form in Fig. 3A strongly resembles plasmonic standing waves in graphene (*20, 21*). The confinement factor λ_{IR}/λ_p reaches 25 in hBN, comparable to that of plasmons in graphene (*20, 21*). Yet these compact polaritons in hBN are able to travel at least 5-10 μm compared to less than 0.5 μm for graphene plasmons. The corresponding loss factor $\gamma = \alpha\kappa/q$ is around 0.055, much smaller than a typical γ in graphene. The low damping of polaritons in our insulating samples is consistent with the absence of the electronic losses, the dominant damping channel in plasmonics. The observed losses can likely be further suppressed by improving the crystallographic order of the crystals.

Data in Fig.1−3 show that phonon polaritons of the desired wavelength and confinement can be engineered by varying the number of atomic layers in hBN by, e.g., exfoliation techniques. Thus, hBN and likely other polar layered materials can be integrated into vdW hetrostructures (*3*) to serve not only as electrically insulating spacers but also as waveguides for weakly damped polaritons capable of traveling over considerable distances. Additionally, the hyperbolic response of few-layer hBN is appealing in the context of unique nano-photonics characteristics of this class of solids (*29*).

References and Notes:

1. C. R. Dean *et al.*, Boron nitride substrates for high-quality graphene electronics. *Nature Nanotechnol.* **5**, 722 (2010). doi:10.1038/nnano.2010.172
2. K. S. Novoselov *et al.*, Two-dimensional atomic crystals. *Proc. Natl. Acad. Sci. U.S.A.* **102**, 10451 (2005). doi:10.1073/pnas.0502848102
3. A. K. Geim, I. V. Grigorieva, Van der Waals heterostructures. *Nature* **499**, 419 (2013). doi:10.1038/nature12385

4. T. Kimura, Y. Tokura, Layered Magnetic Manganites. *Annu. Rev. Mater. Sci.* **30**, 451 (2000). doi:10.1146/annurev.matsci.30.1.451
5. K. F. Mak, C. Lee, J. Hone, J. Shan, T. F. Heinz, Atomically Thin MoS2: A New Direct-Gap Semiconductor. *Phys. Rev. Lett.* **105**, 136805 (2010). doi:10.1103/PhysRevLett.105.136805
6. A. Splendiani *et al.*, Emerging Photoluminescence in Monolayer MoS2. *Nano Lett.* **10**, 1271 (2010). doi:10.1021/nl903868w
7. X. Qi, S. Zhang, Topological insulators and superconductors. *Rev. Mod. Phys.* **83**, 1057 (2011). doi:10.1103/RevModPhys.83.1057
8. L. Britnell et al., Strong Light-Matter Interactions in Heterostructures of Atomically Thin Films. *Science* **340**, 1311 (2013). doi:10.1126/science.1235547
9. S. Z. Butler et al., Progress, Challenges, and Opportunities in Two-Dimensional Materials Beyond Graphene. *ACS Nano* **7**, 2898 (2013). doi:10.1021/nn400280c
10. L. Novotny, B. Hecht, *Principles of Nano-Optics* (Cambridge University Press, Cambridge, England, 2006).
11. J. Renger, S. Grafström, L. M. Eng, R. Hillenbrand, Resonant light scattering by near-field-induced phonon polaritons. *Phys. Rev. B* **71**, 075410 (2005). doi:10.1103/PhysRevB.71.075410
12. S. Shen, A. Narayanaswamy, G. Chen, Surface Phonon Polaritons Mediated Energy Transfer between Nanoscale Gaps. *Nano Lett.* **9**, 2909 (2009). doi:10.1021/nl901208v
13. T. Feurer, J. C. Vaughan, K. A. Nelson, Spatiotemporal Coherent Control of Lattice Vibrational Waves. *Science* **299**, 374 (2003). doi:10.1126/science.1078726
14. Y. De Wilde et al., Thermal radiation scanning tunnelling microscopy. *Nature* **444**, 740 (2006). doi:10.1038/nature05265
15. A. Huber, N. Ocelic, D. Kazantsev, R. Hillenbrand, Near-field imaging of mid-infrared surface phonon polariton propagation. *Appl. Phys. Lett.* **87**, 081103 (2005). doi:10.1063/1.2032595
16. T. Taubner et al., Near-Field Microscopy Through a SiC Superlens. *Science* **313**, 1595 (2006). doi:10.1126/science.1131025
17. G. Shvets, Photonic approach to making a material with a negative index of refraction. *Phys. Rev. B* **67**, 035109 (2003). doi:10.1103/PhysRevB.67.035109
18. J. A. Schuller, R. Zia, T. Taubner, M. L. Brongersma, Dielectric Metamaterials Based on Electric and Magnetic Resonances of Silicon Carbide Particles. *Phys. Rev. Lett.* **99**, 107401 (2007). doi:10.1103/PhysRevLett.99.107401
19. Materials and methods are available as supplementary material on *Science* Online.
20. J. Chen et al., Optical nano-imaging of gate-tunable graphene plasmons. *Nature* **487**, 77 (2012). doi:10.1038/nature11254
21. Z. Fei et al., Gate-tuning of graphene plasmons revealed by infrared nano-imaging. *Nature* **487**, 82 (2012). doi:10.1038/nature11253

22. F. Keilmann, S. Amarie, Mid-infrared Frequency Comb Spanning an Octave Based on an Er Fiber Laser and Difference-Frequency Generation. *J. Infrared Millim. Te.* **33**, 479 (2012). doi:10.1007/s10762-012-9894-x

23. J. M. Atkin, S. Berweger, A. C. Jones, M. B. Raschke, Nano-optical imaging and spectroscopy of order, phases, and domains in complex solids. *Adv. Phys.* **61**, 745 (2012). doi:10.1080/00018732.2012.737982

24. Z. Fei et al., Infrared Nanoscopy of Dirac Plasmons at the Graphene-SiO_2 Interface. *Nano Lett.* **11**, 4701 (2011). doi:10.1021/nl202362d

25. R. Hillenbrand, T. Taubner, F. Keilmann, Phonon-enhanced light–matter interaction at the nanometre scale. *Nature* **418**, 159 (2002). doi:10.1038/nature00899

26. R. Geick, C. H. Perry, G. Rupprecht, Normal Modes in Hexagonal Boron Nitride. *Phys. Rev.* **146**, 543 (1966). doi:10.1103/PhysRev.146.543

27. X. G. Xu, A. E. Tanur, G. C. Walker, Phase Controlled Homodyne Infrared Near-Field Microscopy and Spectroscopy Reveal Inhomogeneity within and among Individual Boron Nitride Nanotubes. *J. Phys. Chem. A* **117**, 3348 (2013). doi:10.1021/jp4008784

28. L. M. Zhang et al., Near-field spectroscopy of silicon dioxide thin films. *Phys. Rev. B* **85**, 075419 (2012). doi:10.1103/PhysRevB.85.075419

29. A. Poddubny, I. Iorsh, P. Belov, and Y.Kivshar, Hyperbolic metamaterials, *Nature Photonics.* **7**, 948 (2013). doi:10.1038/nphoton.2013.243

30. R. Stanley, Plasmonics in the mid-infrared. *Nature Photonics.* **6**, 409 (2012). doi:10.1038/nphoton.2012.161

31. K. Watanabe, T. Taniguchi, H. Kanda, Direct-bandgap properties and evidence for ultraviolet lasing of hexagonal boron nitride single crystal, *Nat. Mater.* **3**, 404 (2004). doi:10.1038/nmat1134

32. R. V. Gorbachev et al., Hunting for Monolayer Boron Nitride: Optical and Raman Signatures. *Small* 7, 465 (2011). doi:10.1002/smll.201001628

33. D. Golla et al., Optical thickness determination of hexagonal boron nitride flakes. *Appl. Phys. Lett.* **102**, 161906 (2013). doi:10.1063/1.4803041

34. S. V. Ordin, B. N. Sharupin, M. I. Fedorov, Normal lattice vibrations and the crystal structure of anisotropic modifications of boron nitride. *Semiconductors* **32**, 924 (1998). doi:10.1134/1.1187516

35. E. Franke et al., Phase and microstructure investigations of boron nitride thin films by spectroscopic ellipsometry in the visible and infrared spectral range. *J. Appl. Phys.* **82**, 2906 (1997). doi:10.1063/1.366123

36. E. Franke et al., *In situ* infrared and visible-light ellipsometric investigations of boron nitride thin films at elevated temperatures. *J. Appl. Phys.* **84**, 526 (1998). doi:10.1063/1.368083

37. Y. Cai, L. Zhang, Q. Zeng, L. Cheng, Y. Xu, Infrared reflectance spectrum of BN calculated from first principles. *Solid State Commun.* **141**, 262 (2007). doi:10.1016/j.ssc.2006.10.040

38. N. Ohba, K. Miwa, N. Nagasako, A. Fukumoto, First-principles study on structural, dielectric, and dynamical properties for three BN polytypes. *Phys. Rev. B* **63**, 115207 (2001). doi:10.1103/PhysRevB.63.115207

39. T. Kuzuba, K. Era, T. Ishii, T. Sato, A low frequency Raman-active vibration of hexagonal boron nitride. *Solid State Commun.* **25**, 863 (1978). doi:10.1016/0038-1098(78)90288-0

40. R. J. Nemanich, S. A. Solin, R. M. Martin, Light scattering study of boron nitride microcrystals. *Phys. Rev. B* **23**, 6348 (1981). doi:10.1103/PhysRevB.23.6348

41. J. Lekner, Reflection ellipsometry of uniaxial crystals. *J. Opt. Soc. Am. A* **14**, 1359 (1997). doi:10.1364/JOSAA.14.001359

42. K. H. Michel, B. Verberck, Theoretical phonon dispersions in monolayers and multilayers of hexagonal boron-nitride. *Phys. Status Solidi B*, **246**, 2802 (2009). doi:10.1002/pssb.200982307

Supplementary Materials

www.sciencemag.org

Materials and Methods

Supplementary Text

Figs. S1 to S5

References (*31-42*)

Acknowledgments: Work at UCSD was supported by DOE-BES. The development of nano-FTIR at UCSD is supported by ONR, DOE, AFOSR and NSF. P. J-H acknowledges support from AFOSR grant number FA9550-11-1-0225. A. S. R. acknowledges DOE grant DE-FG02-08ER46512, and ONR grant MURI N00014-09-1-1063. M. T. and G. D. are supported by NASA. A. H. C. N. acknowledges NRF-CRP award (R-144-000-295-281). A.Z., W.G., and W.R. acknowledge support from the Director, Office of Energy Research, BES,Materials Sciences and Engineering Division, of the U.S. DOE under contract no. DE-AC02- 05CH11231, which provided for preparation and characterization of the BN, and from the ONR, which provided for substrate transfer technique. F.K. is a cofounder of Neaspec, producer of the s-SNOM apparatus used in this study.

Fig. 1. **Real-space imaging of surface phonon polaritons on hBN**. (**A**) Schematics. Arrows denote the incident and back-scattered IR light. Concentric yellow circles illustrate the phonon polariton waves launched by the AFM tip and reflected by the two edges of a tapered hBN crystal. (**B** and **D**-**F**) Infrared near-field images of the normalized amplitude $s(\omega)$ defined in the text and taken at different IR frequencies (hBN thickness in (B-F) d = 256 nm). (**C**) Simulation of the phonon polariton interference pattern (*19*). (**G**) Phonon polaritons probed in a 3 layer (left) and 4 layer (right) hBN crystals. White dashed line tracks the hBN edges according to the AFM topography. Scale bars: 800 nm.

Fig. 2. The surface phonon polariton dispersion and nano-FTIR spectra. (**A**) Schematics of a nano-FTIR line scan across the hBN crystal. Arrows denote the incident and back-scattered IR beam spanning 1350−1600 cm^{-1}. Polaritonic waves are launched (green) by AFM tip and then reflected (orange) by hBN edge at L = 0. (**B**) Polaritonic features detected in a single line scan in (A). The normalized scattering amplitude spectra $s(\omega)$ is plotted in the false color scale. White dashed line at L = 0 marks the edge of the hBN crystal (thickness d = 134 nm). Triangles: fringe maxima extracted from monochromatic imaging similar to Fig. 1. (**C**) Nano-FTIR spectra at three representative locations along the line scan marked in (B). The peaks marked by the arrows correspond to the dominant polariton interference fringe. (**D**) Phonon polariton features as probed via line scans for ultra-thin hBN crystals with d = 3.8 nm (left) and d = 8.8 nm (right). (**E**) The dispersion relation of phonon polaritons in hBN. Triangles: data from monochromatic imaging in Fig. 1; dots: the nano-FTIR results from (B). The data are superimposed on a false color plot of calculated Im r_p (*19*) the black dashed lines are from Eq. 1. The straight line on the left represents the light line. (**F**) Nano-FTIR spectrum $s(\omega)$ for the hBN crystal (Fig. 1 A-F) taken away from the sample edges. The filled (green) part of the data corresponds to hBN's hyperbolic region where $\mathrm{Re}\,\varepsilon_{\perp} \cdot \mathrm{Re}\,\varepsilon_{//} < 0$.

Fig. 3. The evolution of the phonon polariton wavelength and amplitude with the thickness of hBN crystals. (**A**) Line profiles of the scattering amplitude $s(\omega)$ at 1560 cm^{-1} for hBN crystals with d = 154, 237 and 256 nm. Arrows indicate the polariton wavelength. (**B**) Near-field image and (**C**) phonon polariton line profiles for few-layer hBN crystals. White dashed line in (B) tracks the sample boundary. (**D**) Calculated dispersion relation of the l = 0 branch of the phonon polaritons in hBN for various crystal thicknesses. TO and LO frequencies are marked with blue dashed lines. (**E**) Dots: the wavelength of phonon polaritons probed at 1560 cm^{-1} for crystals with different thickness. Red line: calculated thickness-dependence relation. Inset: thickness-dependence relation probed at 1400cm^{-1} for ultra-thin hBN crystals. See (*19*) for details. (**F**) Calculated loss factor for phonon polaritons. Scale bar in (B): 400nm.

Figure 1

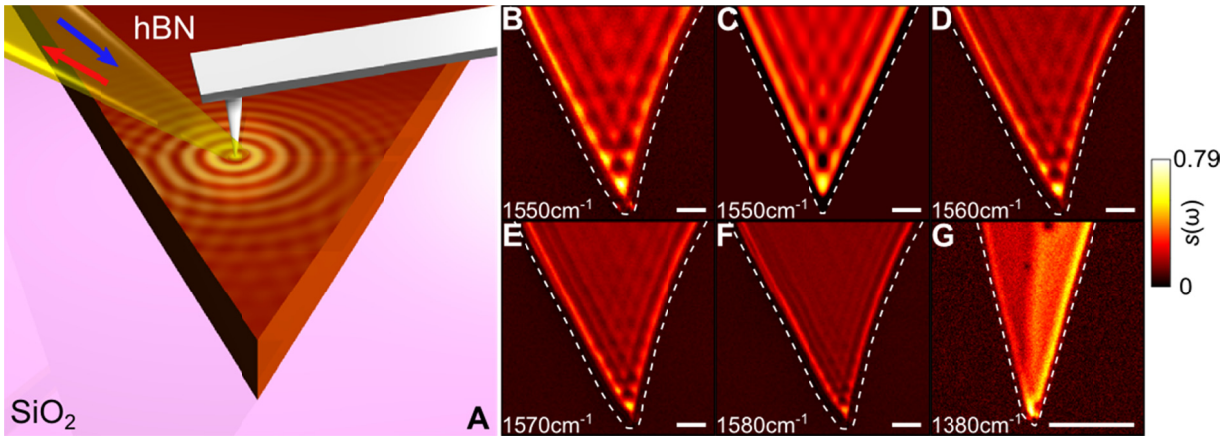
hBN
SiO2
A
B
C
D
E
F
G
1550cm-1
1550cm-1
1560cm-1
1570cm-1
1580cm-1
1380cm-1
0.79
s(ω)
0

Figure 2

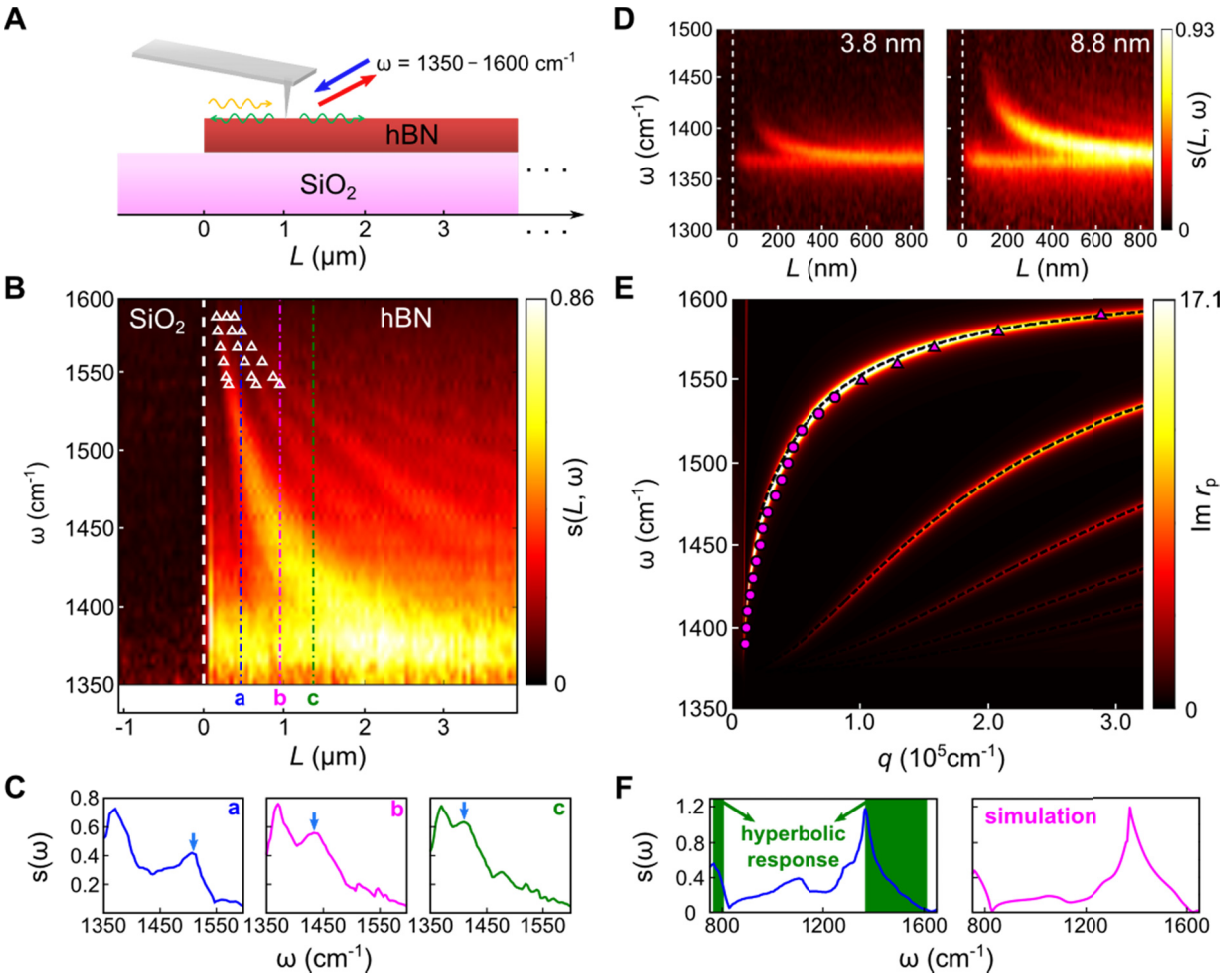
A
ω = 1350 – 1600 cm-1
hBN
SiO2
L (μm)
B
SiO2
hBN
ω (cm-1)
s(L, ω)
0.86
0
a
b
c
L (μm)
C
s(ω)
a
b
c
ω (cm-1)
D
3.8 nm
8.8 nm
ω (cm-1)
L (nm)
s(L, ω)
0.93
0
E
ω (cm-1)
q (10^5cm-1)
Im rp
17.1
0
F
s(ω)
hyperbolic response
simulation
ω (cm-1)

Figure 3

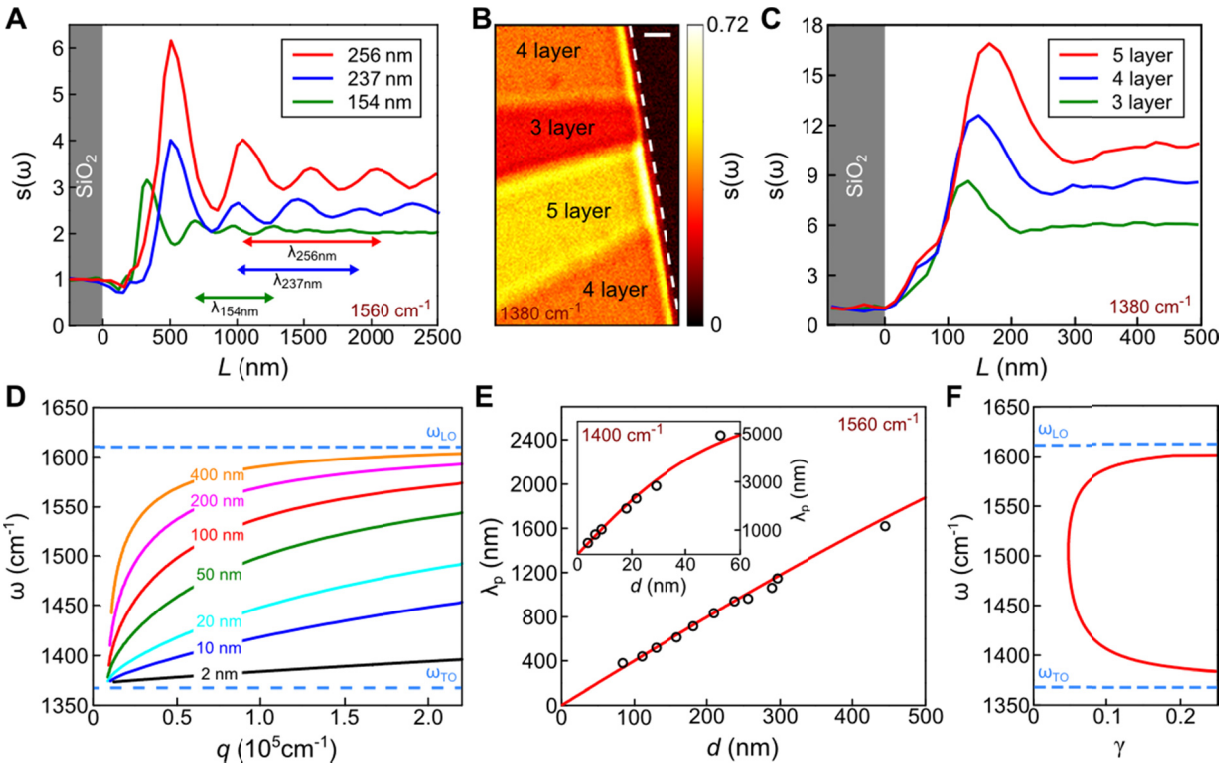
A
B
C
D
E
F
256 nm
237 nm
154 nm
s(ω)
SiO2
L (nm)
λ256nm
λ237nm
λ154nm
1560 cm-1
4 layer
3 layer
5 layer
4 layer
0.72
0
1380 cm-1
5 layer
4 layer
3 layer
ω (cm-1)
ωLO
ωTO
400 nm
200 nm
100 nm
50 nm
20 nm
10 nm
2 nm
q (10^5cm-1)
λp (nm)
d (nm)
1400 cm-1
γ